J|A|C|S
ARTICLES
Published on Web 04/01/2003

Mechanisms of Electron-Transfer Oxidation of NADH Analogues and Chemiluminescence. Detection of the Keto and Enol Radical Cations

Shunichi Fukuzumi,* Osamu Inada, and Tomoyoshi Suenobu

Contribution from the Department of Material and Life Science, Graduate School of Engineering, Osaka University, CREST, Japan Science and Technology Corporation (JST), Suita, Osaka 565-0871, Japan

Received December 7, 2002; E-mail: fukuzumi@chem.eng.osaka-u.ac.jp

Abstract: The radical cation of an NADH analogue (BNAH: 1-benzyl-1,4-dihydronicotinamide) has been successfully detected as the transient absorption and ESR spectra in the thermal electron transfer from BNAH to $Fe(bpy)_3^{3+}$ (bpy = 2,2′-bipyridine) and $Ru(bpy)_3^{3+}$. The ESR spectra of the radical cations of BNAH and the dideuterated compound (BNAH-4,4′-d_2) indicate that the observed radical cation is the keto form rather than the enol form in the tautomerization. The deprotonation rate and the kinetic isotope effects of the keto form of $BNAH^{\bullet+}$ were determined from the kinetic analysis of the electron-transfer reactions. In the case of electron transfer from BNAH to $Ru(bpy)_3^{3+}$, the chemiluminescence due to $Ru(bpy)_3^{2+*}$ was observed in the second electron-transfer step from $BNA^{\bullet}$, produced by the deprotonation of the keto form of $BNAH^{\bullet+}$, to $Ru(bpy)_3^{3+}$. The observation of chemiluminescence due to $Ru(bpy)_3^{2+*}$ provides compelling evidence that the Marcus inverted region is observed even for such an *inter*molecular electron-transfer reaction. When BNAH is replaced by 4-*tert*-butylated BNAH (4-*t*-BuBNAH), no chemiluminescence due to $Ru(bpy)_3^{2+*}$ has been observed in the electron transfer from 4-*t*-BuBNAH to $Ru(bpy)_3^{3+}$. This is ascribed to the facile C−C bond cleavage in 4-*t*-$BuBNAH^{\bullet+}$. In the laser flash photolysis of a deaerated MeCN solution of BNAH and $CHBr_3$, the transient absorption spectrum of the enol form of $BNAH^{\bullet+}$ was detected instead of the keto form of $BNAH^{\bullet+}$, and the enol form was tautomerized to the keto form. The rate of intramolecular proton transfer in the enol form to produce the keto form of $BNAH^{\bullet+}$ was determined from the decay of the absorption band due to the enol form and the rise in the absorption band due to the keto form. The kinetic isotope effects were observed for the intramolecular proton-transfer process in the keto form to produce the enol form.

Introduction

The redox chemistry of 1,4-dihydronicotinamide derivatives has attracted considerable interest in terms of the key role of dihydronicotinamide nucleotide coenzymes (NADH) in a number of biological redox processes including respiratory chain.[1,2] NADH acts as the source of two electrons and a proton, which is equivalent to a hydride ion.[3] In many cases, the two-electron oxidation of NADH and analogues is started by an electron transfer to a substrate, when the radical cations of NADH and analogues should be formed.[4−9] NADH radical cations are important reactive intermediates in the redox conversion between NADH and NAD^+ via the sequential transfer of electron, proton, and electron. Gebicki et al. have reported that certain classes of radical cations can undergo spontaneous tautomerization and that such radical cation tautomerization may also occur for

(1) Stryer, L. *Biochemistry*, 3rd ed.; Freeman: New York, 1988; Chapter 17.
(2) (a) Eisner, U.; Kuthan, J. *Chem. Rev.* **1972**, *72*, 1. (b) Stout, D. M.; Meyers, A. I. *Chem. Rev.* **1982**, *82*, 223. (c) Kellog, R. M. *Angew. Chem., Int. Ed. Engl.* **1984**, *96*, 769.
(3) (a) Kreevoy, M. M.; Ostovic, D.; Lee, I.-S. H.; Binder, D. A.; King, G. W. *J. Am. Chem. Soc.* **1988**, *110*, 524. (b) Kim, Y.; Truhlar, D. G.; Kreevoy, M. M. *J. Am. Chem. Soc.* **1991**, *113*, 7837. (c) Lee, I.-S. H.; Jeoung, E. H.; Kreevoy, M. M. *J. Am. Chem. Soc.* **1997**, *119*, 2722.
(4) (a) Fukuzumi, S.; Tanaka, T. In *Photoinduced Electron Transfer*; Fox, M. A., Chanon, M., Eds.; Elsevier: Amsterdam; 1988; Part C, Chapter 10. (b) Fukuzumi, S. In *Advances in Electron-Transfer Chemistry*; Mariano, P. S., Ed.; JAI press: Greenwich, CT, 1992; pp 67−175. (c) He, G.-X.; Blasko, A.; Bruice, T. C. *Bioorg. Chem.* **1993**, *21*, 423. (d) Ohno, A. *J. Phys. Org. Chem.* **1995**, *8*, 567.
(5) (a) Fukuzumi, S.; Nishizawa, N.; Tanaka, T. *J. Org. Chem.* **1984**, *49*, 3571. (b) Fukuzumi, S.; Koumitsu, S.; Hironaka, K.; Tanaka, T. *J. Am. Chem. Soc.* **1987**, *109*, 305 and references therein.
(6) (a) Fukuzumi, S.; Hironaka, K.; Tanaka, T. *J. Am. Chem. Soc.* **1983**, *105*, 4722. (b) Fukuzumi, S.; Ohkubo, K.; Tokuda, Y.; Suenobu, T. *J. Am. Chem. Soc.* **2001**, *122*, 4286. (c) Fukuzumi, S.; Suenobu, T.; Patz, M.; Hirasaka, T.; Itoh, S.; Fujitsuka, M.; Ito, O. *J. Am. Chem. Soc.* **1998**, *120*, 8060. (d) Fukuzumi, S.; Mochizuki, S.; Tanaka, T. *J. Am. Chem. Soc.* **1989**, *111*, 1497. (e) Liu, Y. C.; Li, B.; Guo, Q. X. *Tetrahedron* **1995**, *51*, 9671. (f) Ohno, A.; Ishikawa, Y.; Yamazaki, N.; Okamura, M.; Kawai, Y. *J. Am. Chem. Soc.* **1998**, *120*, 1186.
(7) (a) Powell, M. F.; Bruice, T. C. *J. Am. Chem. Soc.* **1983**, *105*, 1014, 7139. (b) Chipman, D. M.; Yaniv, R.; van Eikeren, P. *J. Am. Chem. Soc.* **1980**, *102*, 3244. (c) Almarsson, Ö.; Sinha, A.; Gopinath, E.; Bruice, T. C. *J. Am. Chem. Soc.* **1993**, *115*, 7093.
(8) (a) Cheng, J.-P.; Lu, Y.; Zhu, X. Q.; Mu, L. J. *J. Org. Chem.* **1998**, *63*, 6108. (b) Ohno, A.; Ishikawa, Y.; Yamazaki, N.; Okamura, M.; Kawai, Y. *J. Am. Chem. Soc.* **1998**, *120*, 1186. (c) Pestovsky, O.; Bakac, A.; Espenson, J. H. *J. Am. Chem. Soc.* **1998**, *120*, 13422. (d) Pestovsky, O.; Bakac, A.; Espenson, J. H. *Inorg. Chem.* **1998**, *37*, 1616. (e) Carlson, B. W.; Miller, L. L. *J. Am. Chem. Soc.* **1985**, *107*, 479. (f) Miller, L. L.; Valentine, J. R. *J. Am. Chem. Soc.* **1988**, *110*, 3982.
(9) (a) Anne, A.; Fraoura, S.; Grass, V.; Moiroux, J.; Savéant, J.-M. *J. Am. Chem. Soc.* **1998**, *120*, 2951. (b) Anne, A.; Moiroux, J.; Savéant, J.-M. *J. Am. Chem. Soc.* **1993**, *115*, 10224. (c) Anne, A.; Hapiot, P.; Moiroux, J.; Neta, P.; Savéant, J.-M. *J. Am. Chem. Soc.* **1992**, *114*, 4694.

10.1021/ja029623y CCC: $25.00

Scheme 1

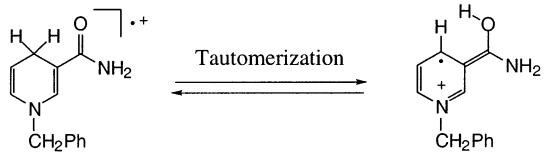

radical cations generated from NADH model compounds (Scheme 1).[10,11]

The transient absorption spectrum of the radical cation of NADH in an aqueous solution has been detected using biphotonic one-electron oxidation of NADH upon laser excitation, exhibiting an absorption maximum at 540 nm.[12] Similar transient absorption bands were reported for NADH model compounds upon laser photolysis of an NADH model compound with an electron acceptor.[13] We have previously reported the formation of radical cations of NADH model compounds in the one-electron oxidation of NADH model compounds with one-electron oxidants and the deprotonation rates of the radical cations.[5b,14] However, definitive assignment of radical cations of NADH model compounds has yet to be made. In addition, there has been no report on the ESR spectra of radical cations of NADH analogues containing a nicotinamide moiety, although ESR spectra of radical cations of dihydroacridine derivatives which do not have a nicotinamide moiety have been fully characterized.[15] The ESR detection of radical cations of NADH analogues would provide definitive information on the structure of the radical cation as to whether it is the keto form or the enol form.

On the other hand, NADH is known to produce chemiluminescence when reacted with $Ru(bpy)_3^{3+}$ (bpy = 2,2′-bipyridine).[16] Such chemiluminescence has been utilized for the determination of other analytes which consume or produce these coenzymes.[17] However, the mechanism of chemiluminescence has yet to be clarified.

We report herein the detection of both the keto and the enol forms of radical cations of NADH analogues in photoinduced electron-transfer reactions using the laser flash technique.[18] The dynamics of keto−enol tautomerization has been successfully monitored to determine the intramolecular proton-transfer rate and the kinetic isotope effect. The thermal electron-transfer mechanism of NADH as well as the chemiluminescence mechanism in the electron-transfer reactions with $Ru(bpy)_3^{3+}$ have been clarified by detailed kinetic analysis. We have also succeeded in detecting the ESR spectra of the keto form of radical cations of NADH analogues. Thus, the present study provides comprehensive electron-transfer mechanisms of NADH analogues.

Experimental Section

Material. Preparation of 1-benzyl-1,4-dihydronicotinamide (BNAH) was described previously.[5b] The dideuterated compound, 1-benzyl-1,4-dihydro [4,4′-$^2H_2$] nicotinamide (BNAH-4,4′-d_2), was prepared from monodeuterated compound (BNAH-4-d_1)[19] by three cycles of oxidation with *p*-chloranil in dimethylformamide and reduction with dithionite in deuterium oxide.[20] The 4-*tert*-butylated and 4-ethylated BNAH (4-*t*-BuBNAH and 4-EtBNAH) were prepared by the Grignard reaction with BNA^+Cl^- and purified by recrystallization from ethanol.[21,22] Tris(2,2′-bipyridyl)ruthenium(III) hexafluorophosphate [$Ru(bpy)_3(PF_6)_3$] and tris(2,2′-bipyridyl)iron(III) hexafluorophosphate [$Fe(bpy)_3(PF_6)_3$] were prepared according to the literature.[23] Tris(2,2′-bipyridyl)ruthenium(II) chloride hexahydrate [$Ru(bpy)_3^{2+}$] and bromoform ($CHBr_3$) were obtained from Aldrich. Acetonitrile (MeCN) and propionitrile (EtCN) as solvents were purified and dried by the standard procedure.[24]

Stopped-Flow Measurements. The transient absorption spectra in the oxidation of BNAH (BNAH-4,4′-d_2) (1.0×10^{-4} M) or 4-*t*-BuBNAH (1.0×10^{-4} M) with $Fe(bpy)_3^{3+}$ (1.5×10^{-4} M) were measured using a UNISOKU RSP-601 stopped-flow rapid scan spectrophotometer equipped with the MOS-type high sensitive photodiode array under deaerated conditions. The gate time for the measurement was set at 2 ms. Typically, deaerated MeCN solutions were transferred to the spectrophotometric cell by means of a glass syringe which had earlier been purged with a stream of argon. The transient absorption spectra in the oxidation of BNAH (BNAH-4,4′-d_2) (6.7×10^{-5} M) with $Ru(bpy)_3^{3+}$ (7.5×10^{-5} M) were measured in the same way.

ESR Measurements. The ESR measurements were performed on a JEOL JES-FA100 ESR spectrometer. Deaerated MeCN solutions of BNAH (BNAH-4,4′-d_2) (8.3×10^{-3} M) and $Fe(bpy)_3^{3+}$ (1.0×10^{-2} M) under an atmospheric pressure of argon were mixed in a flat ESR cell by using a JEOL ES-EMCNT1 rapid mixing flow apparatus. The flow rate was 1.9 $cm^3\ s^{-1}$, and the mixing time before reaching the ESR cell is about several hundred milliseconds. The decay of the ESR signal was measured at a fixed magnetic field, when the flow was stopped. The ESR spectra were recorded under nonsaturating microwave power conditions. The magnitude of modulation was chosen to optimize the resolution and the signal-to-noise (S/N) ratio of the observed spectra. The *g* value and hyperfine splitting constants (hfc) were calibrated by using an Mn^{2+} marker.

Chemiluminescence. The steady-state chemiluminescence spectrum was measured using a SHIMADZU spectrofluorophotometer (RF-5000). A deaerated MeCN solution of $Ru(bpy)_3^{3+}$ (1.0×10^{-2} M) was injected into a deaerated solution of BNAH (5.0×10^{-2} M) using a Harvard Apparatus UL STD 3101-1 syringe pump with the constant flow rate of 9 $\mu L\ min^{-1}$. Decay rates of chemiluminescence were measured by mixing deaerated solutions of BNAH (BNAH-4,4′-d_2) (5.0×10^{-4} M) and deaerated solutions of $Ru(bpy)_3^{3+}$ (1.0×10^{-3} M) using a

(10) (a) Gebicki, J.; Bally, T. *Acc. Chem. Res.* **1997**, *30*, 477. (b) Gebicki, J. *Pure Appl. Chem.* **1995**, *67*, 55. (c) Gebicki, J.; Marcinek, A.; Adamus, J.; Paneth, P.; Rogowski, J. *J. Am. Chem. Soc.* **1996**, *118*, 691.
(11) (a) Marcineck, A.; Adamus, J.; Huben, K.; Gebicki, J.; Bartczak, T. J.; Bednarek, P.; Bally, T. *J. Am. Chem. Soc.* **2000**, *122*, 437. (b) Marcinek, A.; Rogowski, J.; Adamus, J.; Gebicki, J.; Benarek, P.; Bally, T. *J. Phys. Chem. A* **2000**, *104*, 718.
(12) (a) Czochralska, B.; Lindqvist, L. *Chem. Phys. Lett.* **1983**, *101*, 297. (b) Lindqvist, L.; Czochralska, B.; Grigorov, I. *Chem. Phys. Lett.* **1985**, *119*, 494.
(13) Anne, A.; Hapiot, P.; Moiroux, J.; Neta, P.; Savéant, J.-M. *J. Am. Chem. Soc.* **1992**, *114*, 4694.
(14) (a) Fukuzumi, S.; Kondo, Y.; Tanaka, T. *Chem. Lett.* **1982**, 1591. (b) Fukuzumi, S.; Kondo, Y.; Tanaka, T. *J. Chem. Soc., Perkin Trans. 2* **1984**, 673.
(15) Fukuzumi, S.; Tokuda, Y.; Kitano, T.; Okamoto, T.; Otera, J. *J. Am. Chem. Soc.* **1993**, *115*, 8960.
(16) (a) Downey, T. M.; Nieman, T. A. *Anal. Chem.* **1992**, *64*, 261. (b) Uchikura, K.; Kirisawa, M. *Chromatography* **1992**, *13*, 257.
(17) (a) Martin, A. F.; Nieman, T. A. *Anal. Chim. Acta* **1993**, *281*, 475. (b) Yokoyama, K.; Sasaki, K.; Ikebukuro, K.; Takeuchi, I.; Karube, Y.; Tokitsu, Y.; Masuda, Y. *Talanta* **1994**, *41*, 1035. (c) Jameison, F.; Sanchez, R. I.; Dong, L.; Leland, J. K.; Yost, D.; Martin, M. T. *Anal. Chem.* **1996**, *68*, 1298. (d) Gerardi, R. D.; Barnett, N. W.; Lewis, S. W. *Anal. Chim. Acta* **1999**, *378*, 1. (e) Lee, W.-Y.; Nieman, T. A. *Anal. Chem.* **1995**, *67*, 1789.
(18) A part of the present results has appeared as a preliminary communication, see: Fukuzumi, S.; Inada, O.; Suenobu, T. *J. Am. Chem. Soc.* **2002**, *124*, 14538.
(19) (a) Anderson, A. G., Jr.; Berkelhammer, G. *J. Am. Chem. Soc.* **1958**, *80*, 992. (b) Mauzerall, D.; Westheimer, F. H. *J. Am. Chem. Soc.* **1955**, *77*, 2261.
(20) Caughey, W.; Schellenberg, K. A. *J. Org. Chem.* **1966**, *31*, 1978.
(21) Anne, A. *Heterocycles* **1992**, *34*, 2331.
(22) Takada, N.; Itoh, S.; Fukuzumi, S. *Chem. Lett.* **1996**, 1103.
(23) DeSimone, R. E.; Drago, R. S. *J. Am. Chem. Soc.* **1970**, *92*, 2343.
(24) Perrin, D. D.; Armarego, W. L. F. *Purification of Laboratory Chemicals*; Butterworth-Heinemann: Oxford, 1988.

UNISOKU RSP-601 stopped-flow rapid scan spectrophotometer equipped with the MOS-type high sensitive photodiode array and with the light source switched off under deaerated conditions. The gate time for the measurement was set at 2 ms. Typically, deaerated MeCN solutions were transferred to the spectrophotometric cell by means of a glass syringe which had earlier been purged with a stream of argon.

Laser Flash Photolysis Measurements. The measurements of transient absorption spectra in the photooxidation of BNAH, BNAH-4,4′-d_2, 4-EtBNAH, and 4-*t*-BuBNAH with $CHBr_3$ were performed according to the following procedures. The degassed EtCN solution containing BNAH (BNAH-4,4′-d_2) (4.0×10^{-4} M), 4-EtBNAH (4.0×10^{-4} M), or 4-*t*-BuBNAH (4.0×10^{-4} M) and $CHBr_3$ (0.25 M) was excited by a Nd:YAG laser (Continuum, SLII-10, 4−6 ns fwhm) at $\lambda = 355$ nm with a power of 20 mJ per pulse. The transient absorption spectra (Figures 8a, S5, and S6) for the photoinduced electron-transfer reactions were measured by using a continuous Xe-flash lamp (EPS, XN-20MS, 12 mJ/pulse) as a probe light and a photodiode array S3904-1024F with gated image intensifier C2925-01 (Hamamatsu Photonics) as a detector. Time courses of the transient absorption spectra were measured by using a continuous Xe-lamp (150 W) and an InGaAs-PIN photodiode (Hamamatsu 2949) as a probe light and a detector, respectively. The output from the photodiodes and a photomultiplier tube was recorded with a digitizing oscilloscope (Tektronix, TDS3032, 300 MHz). The transient spectra were recorded using fresh solutions in each laser excitation. The measurements of transient absorption spectra in the photooxidation of BNAH and 4-*t*-BuBNAH with $Ru(bpy)_3^{2+}$ were performed according to the following procedures. The degassed MeCN solution containing BNAH (3.0×10^{-3} M) or 4-*t*-BuBNAH (1.0×10^{-2} M) and $Ru(bpy)_3^{2+}$ (1.0×10^{-4} M) was excited by a Panther OPO pumped by Nd:YAG laser (Continuum, SLII-10, 4−6 ns fwhm) at $\lambda = 450$ nm with the power of 10 mJ per pulse. The photoinduced electron-transfer reactions were monitored by using a continuous Xe-lamp (150 W) and an InGaAs-PIN photodiode (Hamamatsu 2949) as a probe light and a detector, respectively. The output from the photodiodes and a photomultiplier tube was recorded with a digitizing oscilloscope (Tektronix, TDS3032, 300 MHz).

Theoretical Calculation. Density-functional theory (DFT) calculations were performed on a COMPAQ DS20E computer. Geometry optimizations were carried out using the B3LYP functional and 6-31G* basis set[25,26] with the unrestricted Hartree−Fock (UHF) formalism as implemented in the Gaussian 98 program.[27]

Results and Discussion

Thermal Electron-Transfer Oxidation of BNAH. Thermal electron-transfer oxidation of an NADH analogue (BNAH) was examined using $Fe(bpy)_3^{3+}$ and $Ru(bpy)_3^{3+}$ as one-electron oxidants in MeCN. The initial electron transfer from BNAH to $Fe(bpy)_3^{3+}$ and $Ru(bpy)_3^{3+}$ is too rapid to be monitored using a stopped-flow technique. This is consistent with the largely negative free energy change of electron transfer from BNAH (E_{ox}^0 vs SCE = 0.57 V)[5b] to $Fe(bpy)_3^{3+}$ (E_{red}^0 vs SCE = 1.06 V)[28] and $Ru(bpy)_3^{3+}$ (E_{red}^0 vs SCE = 1.24 V).[29] The differential absorption spectra were recorded by subtracting the final absorption spectrum from the observed spectra during the electron-transfer oxidation of BNAH by $Ru(bpy)_3^{3+}$ as shown in Figure 1 (see Supporting Information S1 for the original spectra). The new absorption band at 380 nm appears upon mixing MeCN solutions of BNAH and $Ru(bpy)_3^{3+}$ and disappears accompanied by the appearance of the absorption band at 450 nm due to $Ru(bpy)_3^{2+}$. The absorption band at 380 nm can be assigned to $BNAH^{\bullet+}$. The same absorption band due to $BNAH^{\bullet+}$ was observed in the electron-transfer oxidation of BNAH by $Fe(bpy)_3^{3+}$.[18] The decay rate of $BNAH^{\bullet+}$ obeys first-order kinetics (Figure 2a), coinciding with the rate of formation of $Fe(bpy)_3^{2+}$ (Figure 2b). When BNAH is replaced by BNAH-4,4′-d_2, the kinetic isotope effects were observed for both the decay rate of $BNAH^{\bullet+}$ and the rate of formation of $Fe(bpy)_3^{2+}$ as shown in Table 1. This indicates that the decay of $BNAH^{\bullet+}$ occurs via deprotonation to produce $BNA^{\bullet}$, which is rapidly oxidized by $Fe(bpy)_3^{3+}$ (Scheme 2).

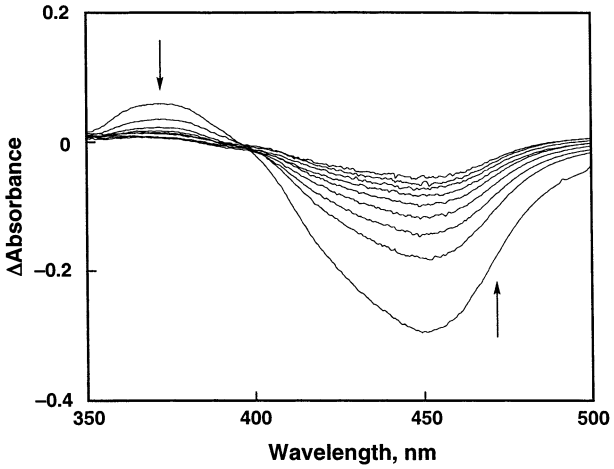

Figure 1. Differential spectral change in thermal electron transfer from BNAH (6.7×10^{-5} M) to $Ru(bpy)_3^{3+}$ (7.5×10^{-5} M) in deaerated MeCN at 298 K; time interval: 20 ms.

Judging from the highly negative oxidation potential of $BNA^{\bullet}$ (E_{ox}^0 vs SCE = −1.08 V), which is equivalent to the reduction potential of BNA^+,[5b] the electron transfer from $BNA^{\bullet}$ to $Fe(bpy)_3^{3+}$ (E_{red}^0 vs SCE = 1.06 V)[28] is highly exergonic, and thus it is expected to be diffusion-limited. In such a case, the rate-limiting step for formation of $Fe(bpy)_3^{2+}$ is the deprotonation from $BNAH^{\bullet+}$ as observed experimentally. The Eyring plots of the deprotonation rate constant (k) of $BNAH^{\bullet+}$ (Figure 3) afforded the activation parameters listed in Table 2.

When BNAH is replaced by 4-*t*-BuBNAH where the hydrogen at the C(4) position is substituted by a *tert*-butyl group, no transient absorption spectrum due to 4-*t*-$BuBNAH^{\bullet+}$ has been detected (see Supporting Information S2). We have previously reported that cleavage of the C(9)−C bond of a radical cation of an NADH analogue, 9-*tert*-butyl-10-methyl-9,10-dihydroacridine [AcrH(*t*-Bu)], occurs selectively rather than the cleavage of the C(9)−H bond in the electron-transfer oxidation of AcrH(*t*-

(25) (a) Becke, A. D. *J. Chem. Phys.* **1993**, *98*, 5648. (b) Lee, C.; Yang, W.; Parr, R. G. *Phys. Rev. B* **1988**, *37*, 785.
(26) Hehre, W. J.; Radom, L.; Schleyer, P. v. R.; Pople, J. A. *Ab Initio Molecular Orbital Theory*; Wiley: New York, 1986.
(27) Frisch, M. J.; Trucks, G. W.; Schlegel, H. B.; Scuseria, G. E.; Robb, M. A.; Cheeseman, J. R.; Zakrzewski, V. G.; Montgomery, J. A., Jr.; Stratmann, R. E.; Burant, J. C.; Dapprich, S.; Millam, J. M.; Daniels, A. D.; Kudin, K. N.; Strain, M. C.; Farkas, O.; Tomasi, J.; Barone, V.; Cossi, M.; Cammi, R.; Mennucci, B.; Pomelli, C.; Adamo, C.; Clifford, S.; Ochterski, J.; Petersson, G. A.; Ayala, P. Y.; Cui, Q.; Morokuma, K.; Malick, D. K.; Rabuck, A. D.; Raghavachari, K.; Foresman, J. B.; Cioslowski, J.; Ortiz, J. V.; Baboul, A. G.; Stefanov, B. B.; Liu, G.; Liashenko, A.; Piskorz, P.; Komaromi, I.; Gomperts, R.; Martin, R. L.; Fox, D. J.; Keith, T.; Al-Laham, M. A.; Peng, C. Y.; Nanayakkara, A.; Gonzalez, C.; Challacombe, M.; Gill, P. M. W.; Johnson, B.; Chen, W.; Wong, M. W.; Andres, J. L.; Gonzalez, C.; Head-Gordon, M.; Replogle, E. S.; Pople, J. A. *Gaussian 98*, revision A.7; Gaussian, Inc.; Pittsburgh, PA, 1998.
(28) Fukuzumi, S.; Nishizawa, N.; Tanaka, T. *Bull. Chem. Soc. Jpn.* **1982**, *55*, 3482.
(29) Fukuzumi, S.; Nakanishi, I.; Tanaka, K.; Suenobu, T.; Tabard, A.; Guilard, R.; Van Caemelbecke, E.; Kadish, K. M. *J. Am. Chem. Soc.* **1999**, *121*, 785.

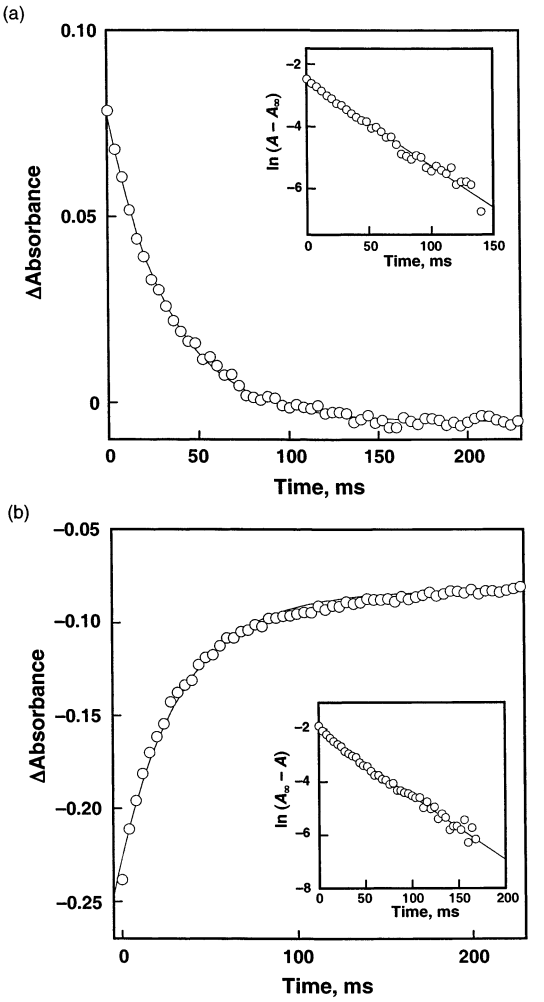

Figure 2. (a) Time course of absorbance change at 380 nm for the reaction of BNAH (1.0×10^{-4} M) with $Fe(bpy)_3^{3+}$ (1.5×10^{-4} M) in deaerated MeCN at 298 K. Inset: First-order plot based on the absorption change at 380 nm. (b) Time course of absorbance change at 520 nm for the reaction of BNAH (1.0×10^{-4} M) with $Fe(bpy)_3^{3+}$ (1.5×10^{-4} M) in deaerated MeCN at 298 K. Inset: First-order plot based on the absorption change at 520 nm.

Table 1. Rate Constants (k) of Deprotonation of $BNAH^{\bullet+}$ and BNAH-4,4′-$d_2^{\bullet+}$ in the Reaction of BNAH or BNAH-4,4′-$d_2^{\bullet+}$ (1.0×10^{-4} M) with $Fe(bpy)_3^{3+}$ (1.5×10^{-4} M) in Deaerated MeCN

T, K	k_H, s^{-1}	k_D, s^{-1}	k_H/k_D
298	24	18	1.3
278	15	9.6	1.5
258	8.5	5.1	1.7
243	6.0	3.1	1.9

Bu) by Fe^{3+} complexes.[15] One-electron oxidation of 4-*t*-BuBNAH is also known to result in the selective C(4)−C bond cleavage of 4-*t*-$BuBNAH^{\bullet+}$ to give *t*-$Bu^{\bullet}$ and BNA^+ (Scheme 3),[6c] both of which have no absorption bands in the visible region. Such an ultrafast carbon−carbon bond cleavage is also known for benzpinacol radical cations.[30] In such a case, two-electron oxidation of 4-*t*-BuBNAH occurs with 2 equiv of $Fe(bpy)_3^{3+}$ (Scheme 3). The second electron transfer from *t*-$Bu^{\bullet}$ (E_{ox}^0 vs SCE = 0.09 V),[31] which is generated via the facile

(30) Bockman, T. M.; Hubig, S. M.; Kochi, J. K. *J. Am. Chem. Soc.* **1998**, *120*, 6542.
(31) Wayner, D. D. M.; McPhee, D. J.; Griller, D. *J. Am. Chem. Soc.* **1988**, *110*, 132.

Scheme 2

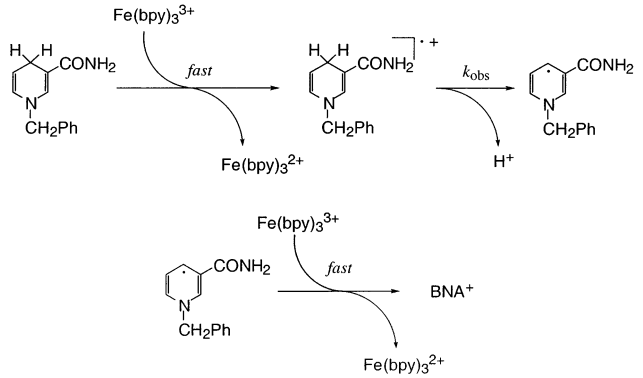

Table 2. Activation Parameters of Deprotonation and Tautomerization of $BNAH^{\bullet+}$ and BNAH-4,4′-$d_2^{\bullet+}$

	$\Delta H^{\ddagger a}$ (kcal mol^{-1})	$\Delta S^{\ddagger a}$ (cal K^{-1} mol^{-1})	$\Delta H^{\ddagger b}$ (kcal mol^{-1})	$\Delta S^{\ddagger b}$ (cal K^{-1} mol^{-1})
$BNAH^{\bullet+}$	3.1	42	1.9	29
BNAH-4,4′-$d_2^{\bullet+}$	4.1	39	2.8	25

[a] Determined by an Eyring plot of deprotonation rates.[18] [b] Determined by an Eyring plot of tautomerization rates.

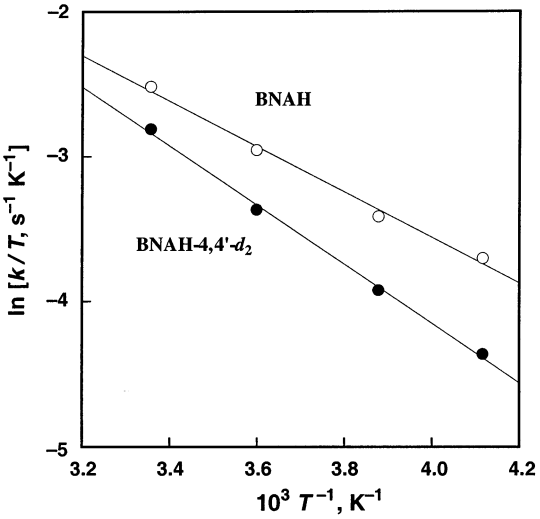

Figure 3. Eyring plots of the deprotonation rate constant (k) of $BNAH^{\bullet+}$ (○) and BNAH-4,4′-$d_2^{\bullet+}$ (●) in deaerated MeCN.

Scheme 3

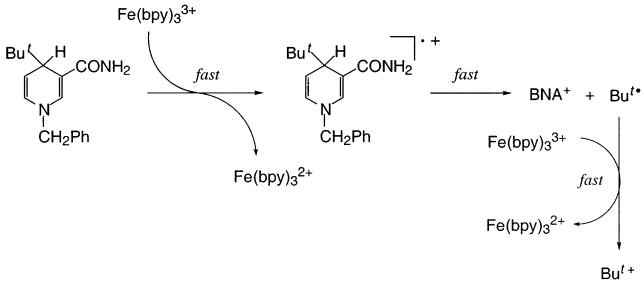

C−C bond cleavage in 4-*t*-$BuBNAH^{\bullet+}$, to $Fe(bpy)_3^{3+}$ (E_{red}^0 vs SCE = 1.06 V)[28] is as rapid as the initial electron transfer from 4-*t*-BuBNAH (E_{ox}^0 vs SCE = 0.71 V)[22] to $Fe(bpy)_3^{3+}$. The two-electron oxidation mechanism of 4-*t*-BuBNAH, including the trapping of the *t*-$Bu^{\bullet}$ radical with oxygen, has previously been reported.[22]

ESR Detection of the Keto Form of $BNAH^{\bullet+}$. The relatively long lifetime of the radical cation of BNAH in Figure 1 enabled

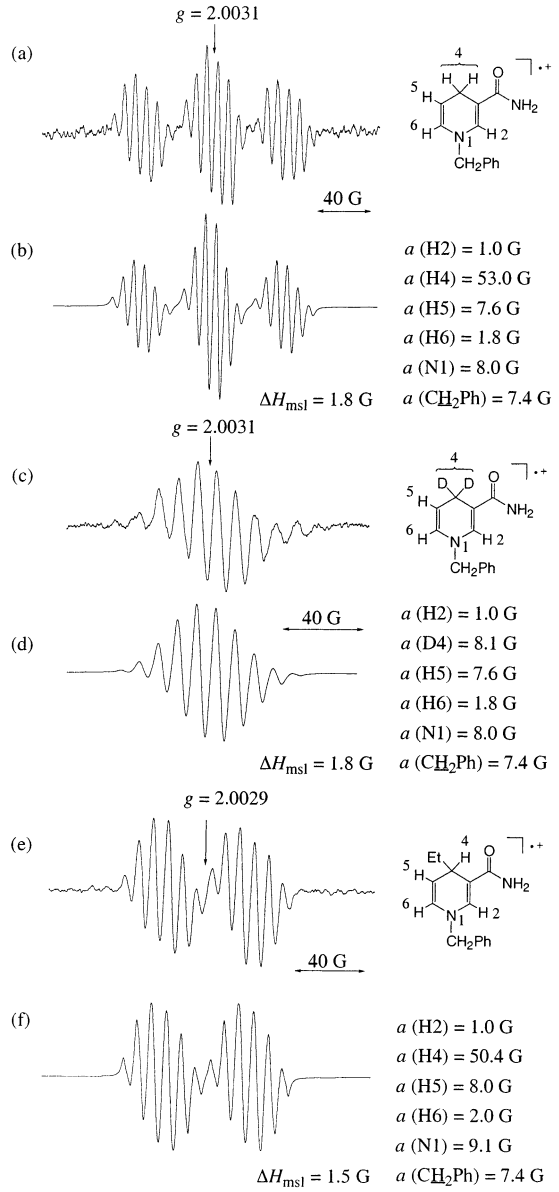

Figure 4. (a) ESR spectrum of the keto form of $BNAH^{\bullet+}$ generated by oxidation of BNAH (8.3×10^{-3} M) with $Fe(bpy)_3^{3+}$ (1.0×10^{-2} M) in deaerated MeCN at 233 K and (b) the computer simulation spectrum with the hfc values. (c) ESR spectrum of the keto form of BNAH-4,4′-$d_2$$^{\bullet+}$ generated by oxidation of BNAH-4,4′-d_2 (8.3×10^{-3} M) with $Fe(bpy)_3^{3+}$ (1.0×10^{-2} M) in deaerated MeCN at 233 K and (d) the computer simulation spectrum with the hfc values. (e) ESR spectrum of the keto form of 4-$EtBNAH^{\bullet+}$ generated by oxidation of 4-EtBNAH (8.3×10^{-3} M) with $Fe(bpy)_3^{3+}$ (1.0×10^{-2} M) in deaerated MeCN at 233 K and (f) the computer simulation spectrum with the hfc values.

us to detect the ESR spectrum for the first time in the electron-transfer oxidation of BNAH with $Fe(bpy)_3^{3+}$ in deaerated MeCN by applying a rapid-mixing ESR technique as shown in Figure 4a.[18]

The *g*-value is 2.0031, which is slightly larger than the free spin value, indicating the contribution of spin−orbit coupling due to electron spin at the nitrogen and oxygen atoms. The hyperfine coupling constants (hfc) are determined by comparison of the observed spectrum with the computer simulated spectrum as shown in Figure 4b. By comparing the hfc values with the spin densities obtained by the DFT calculation,[32] we assigned the hfc values as shown in Figure 4b.[33] Large hfc values (53.0

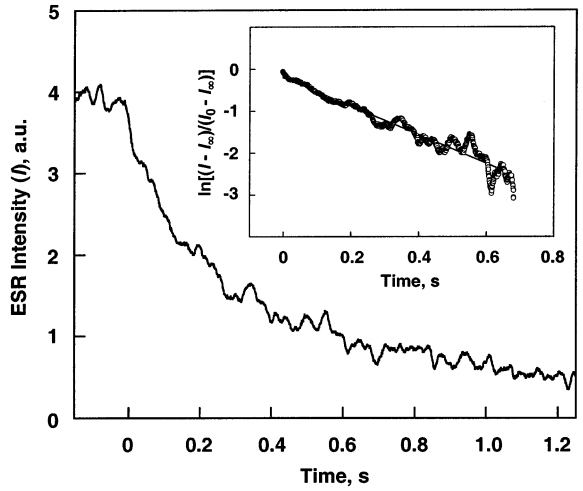

Figure 5. Decay of the ESR signal intensity of $BNAH^{\bullet+}$ at $g = 2.0195$ observed in the reaction of BNAH (8.3×10^{-3} M) with $Fe(bpy)_3^{3+}$ (1.0×10^{-2} M) in deaerated MeCN at 233 K. Inset: First-order plot.

G) are assigned to the two protons at the C(4) position, because the hfc value is significantly larger than the maximum hfc value (23.04 G) of proton bonding to the sp^2 carbon (C(4) in enol form).[34] Such large values at the C4 position are consistent with those of NADH expected by photo-CIDNP experiments,[35] which confirm that $BNAH^{\bullet+}$ detected by ESR is the keto form. Deuterium substitution at these positions permits an experimental verification of the assignment of the observed radical species, because a single deuteron gives a triplet (instead of doublet) hyperfine pattern and the deuteron splitting should decrease by the magnetogyric ratio of proton to deuterium (0.153).[34] In fact, deuterium substitution of two hydrogen atoms at the C(4) of $BNAH^{\bullet+}$ results in drastic changes in the splitting pattern from the spectrum in Figure 4a to that in Figure 4c, where BNAH is substituted by BNAH-4,4′-d_2. The computer simulation spectrum using the same hfc values except for the deuterium ($I = 1$) at the C(4) position, which are reduced by a factor of 0.153, agrees well with the observed ESR spectrum of BNAH-4,4′-$d_2$$^{\bullet+}$ (Figure 4d). Such an agreement confirms the hfc assignment in Figure 4. When 4-ethyl substituted BNAH (4-EtBNAH) was used in place of BNAH, the ESR spectrum of 4-$EtBNAH^{\bullet+}$ was observed at $g = 2.0029$ in the electron-transfer oxidation of 4-EtBNAH with $Fe(bpy)_3^{3+}$ in deaerated MeCN (Figure 4e). The hfc values are assigned as shown in Figure 4f.[33] A large hfc value (50.4 G) assigned to a proton at the C(4) position further confirms that 4-$EtBNAH^{\bullet+}$ exists as the keto form rather than the enol form. In the case of 4-*t*-BuBNAH, no ESR spectrum of 4-*t*-$BuBNAH^{\bullet+}$ was detected due to the facile C−C bond cleavage in 4-*t*-$BuBNAH^{\bullet+}$.[22]

To confirm that the keto form of $BNAH^{\bullet+}$ observed in the ESR spectrum in Figure 4 is the same as that observed in the

(32) (a) Gauld, J. W.; Eriksson, L. A.; Radom, L. *J. Phys. Chem. A* **1997**, *101*, 1352. (b) Lassmann, G.; Eriksson, L. A.; Lendzian, F.; Lubitz, W. *J. Phys. Chem. A* **2000**, *104*, 9144.
(33) The assignment of the hfc values is made by comparison with the hfc values predicted by the DFT calculation (B3LYP functional and 6-31G* basis set). The calculated hfc values are obtained as 1.3 (H2), 57.0 (H4), 9.7 (H5), 1.9 (H6), 12.8 (CH_2Ph), and 8.9 G (N1) for $BNAH^{\bullet+}$, and 1.1 (H2), 52.5 (H4), 9.0 (H5), 2.0 (H6), 11.0 (CH_2Ph), and 8.8 G (N1) for 4-$EtBNAH^{\bullet+}$, which are used for assignment of the observed hfc values.
(34) Weil, J. A.; Bolton, J. R.; Wertz, J. E. *Electron Paramagnetic Resonance: Elementary Theory and Practical Applications*; John Wiley & Sons: New York, 1994.
(35) Hore, P. J.; Volbeda, A.; Dijkstra, K.; Kaptein, R. *J. Am. Chem. Soc*. **1982**, *104*, 6262.

Scheme 4

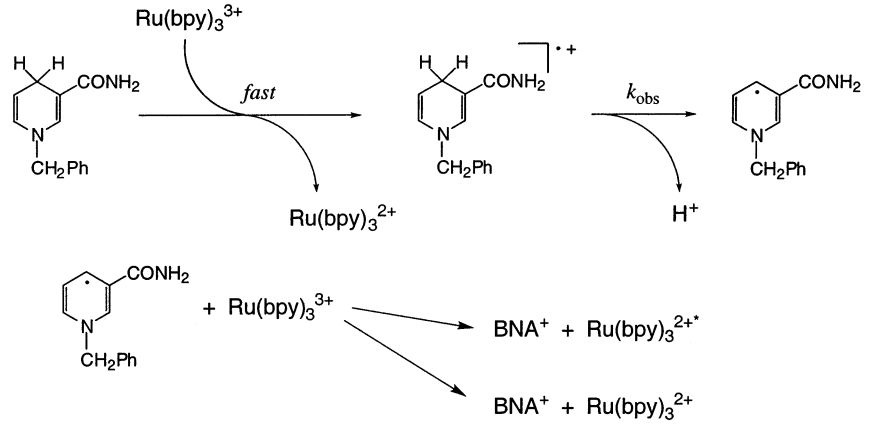

transient absorption spectrum in Figure 1, the decay dynamics of the ESR signal was examined. The decay rate obeyed first-order kinetics as shown in Figure 5, and the first-order decay rate constant (k) at 233 K was determined as 3.4 s^{-1}. This value agrees within experimental error with the extrapolated value from the Eyring plot in Figure 3 for the deprotonation rate constant of $BNAH^{\bullet+}$ ($k_H = 4.0\ s^{-1}$) determined from the decay dynamics of the transient absorption band at $\lambda_{max} = 380$ nm. Such an agreement confirms that the transient species detected by ESR in Figure 4 is the same as that detected by UV−vis in Figure 1 and that both species are definitely assigned to the keto form of $BNAH^{\bullet+}$.[36] However, the λ_{max} value of the keto form of $BNAH^{\bullet+}$ is quite different from the reported λ_{max} value of $NADH^{\bullet+}$ (540 nm) observed in biphotonic one-electron oxidation of NADH upon laser excitation.[12]

Chemiluminescence in Electron Transfer from BNAH to $Ru(bpy)_3^{3+}$. When $Fe(bpy)_3^{3+}$ is replaced by a stronger oxidant, $Ru(bpy)_3^{3+}$, virtually the same electron-transfer mechanism in Scheme 2 is applied to the electron transfer from BNAH to $Ru(bpy)_3^{3+}$ as shown in Scheme 4. In this case, however, the luminescence of $Ru(bpy)_3^{2+}$ ($\lambda_{max} = 610$ nm) is observed during the electron transfer from BNAH to $Ru(bpy)_3^{3+}$ as shown in Figure 6a. The chemiluminescence spectrum in Figure 6a agrees with the emission spectrum of $Ru(bpy)_3^{2+*}$ (* denotes the excited state) (Figure 6b). Figure 7a shows the dynamics of the chemiluminescence observed in the electron transfer from BNAH to $Ru(bpy)_3^{3+}$. As in the case of electron transfer from BNAH to $Fe(bpy)_3^{3+}$, the initial electron transfer from BNAH to $Ru(bpy)_3^{3+}$ is too rapid to be monitored using a stopped-flow technique because of the largely negative free energy change of electron transfer from BNAH (E_{ox}^0 vs SCE = 0.57 V)[5b] to $Ru(bpy)_3^{3+}$ (E_{red}^0 vs SCE = 1.24 V).[29] The chemiluminescence of $Ru(bpy)_3^{2+*}$ is observed upon mixing MeCN solutions of BNAH and $Ru(bpy)_3^{3+}$, and the decay of the luminescence intensity at 610 nm obeys first-order kinetics (see Supporting Information S3), which coincides with the formation rate of $Ru(bpy)_3^{2+}$ monitored at 450 nm (Figure 7a). When BNAH is mixed with $Ru(bpy)_3^{3+}$ in an aqueous solution, BNAH is solubilized into an aqueous solution slowly as the oxidation of BNAH by $Ru(bpy)_3^{3+}$ proceeds. In such a case, the persistent

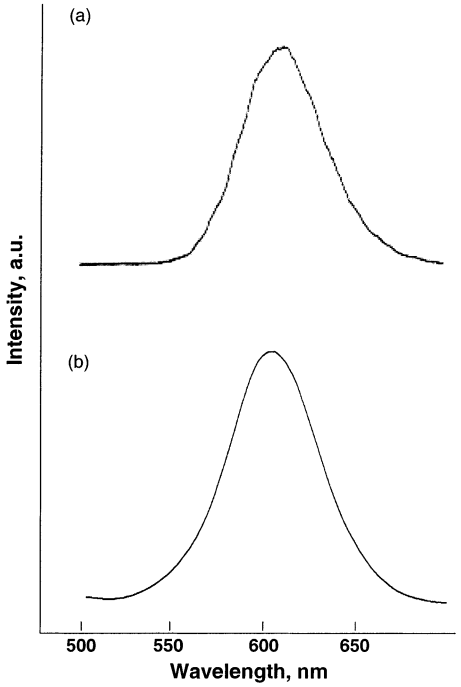

Figure 6. (a) Chemiluminescence spectrum observed during mixing BNAH (5.0×10^{-2} M) with $Ru(bpy)_3^{3+}$ (1.0×10^{-2} M) in deaerated MeCN at 298 K and (b) emission spectrum of $Ru(bpy)_3^{2+*}$ with excitation at 452 nm.

chemiluminescence of $Ru(bpy)_3^{2+*}$ is observed until all BNAH molecules are consumed (see TOC).

When BNAH is replaced by BNAH-4,4′-d_2, the kinetic isotope effects ($k_H/k_D = 1.4$) are observed for both the decay rate of the luminescence intensity and the rate of formation of $Ru(bpy)_3^{2+}$ as shown in Figure 7b. The k_H/k_D value at 298 K agrees well with the value observed for the deprotonation of $BNAH^{\bullet+}$ (Table 1).

According to Scheme 4, the rate of deprotonation of the keto form of $BNAH^{\bullet+}$ is the same as the formation rate of $Ru(bpy)_3^{2+}$. The electron transfer from $BNA^{\bullet}$ (E_{ox}^0 vs SCE = −1.08 V)[5b] to $Ru(bpy)_3^{3+}$ (E_{red}^0 vs SCE = 1.24 V)[29] is highly exergonic ($\Delta G_{et}^0 = -2.32$ eV) when the driving force of electron transfer is larger than the excitation energy of $Ru(bpy)_3^{2+}$ (2.12 eV). In such a case, electron transfer from $BNA^{\bullet}$ to $Ru(bpy)_3^{3+}$ to produce $Ru(bpy)_3^{2+*}$ is still exergonic (−0.20 eV). The initial electron transfer from BNAH to $Ru(bpy)_3^{3+}$ is not exergonic enough to produce $Ru(bpy)_3^{2+*}$. Thus, the

(36) The concentration of $BNAH^{\bullet+}$ detected by the ESR spectrum in Figure 4a is much smaller than the concentration detected by the transient absorption spectrum because of the short lifetime of $BNAH^{\bullet+}$ (0.24 s) and the longer mixing time required for the ESR flow measurements (about several hundreds of milliseconds) than the mixing time for the transient absorption measurements (about several tens of milliseconds).

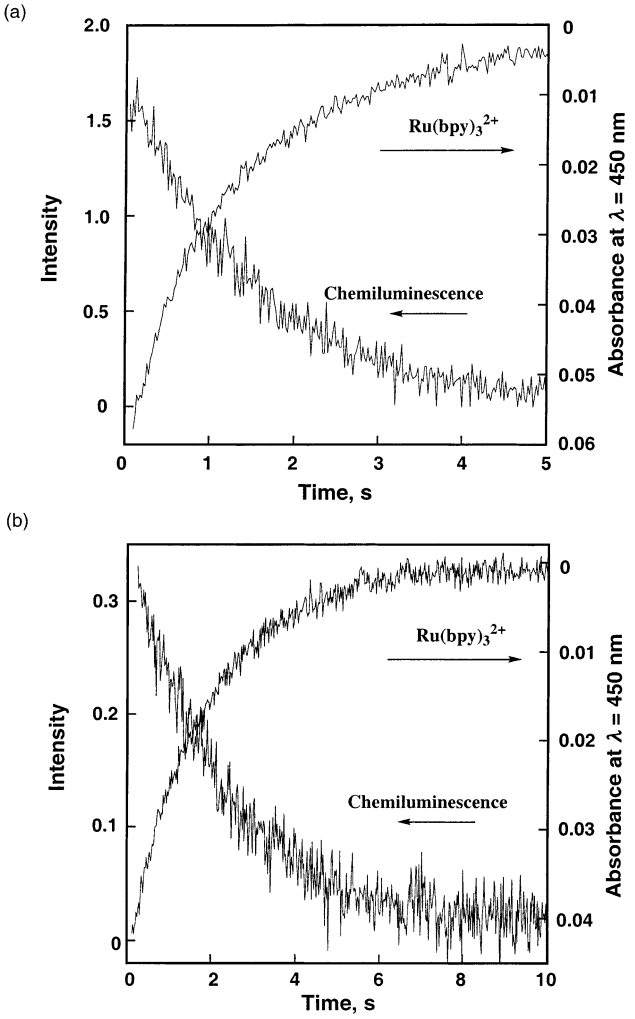

Figure 7. (a) Time courses of emission intensity change at 610 nm and absorption change at 450 nm for the reaction of BNAH (5.0×10^{-4} M) with $Ru(bpy)_3^{3+}$ (1.0×10^{-3} M) in deaerated MeCN at 298 K and (b) time courses of emission intensity change at 610 nm and absorption change at 450 nm for the reaction of BNAH-4,4′-d_2 (5.0×10^{-4} M) with $Ru(bpy)_3^{3+}$ (1.0×10^{-3} M) in deaerated MeCN at 298 K.

observation of the strong $Ru(bpy)_3^{2+*}$ emission indicates that electron transfer from BNA$^\bullet$ to $Ru(bpy)_3^{3+}$ occurs to produce $Ru(bpy)_3^{2+*}$ ($\Delta G_{et}^0 = -0.20$ eV) as well as $Ru(bpy)_3^{2+}$ ($\Delta G_{et}^0 = -2.32$ eV). The occurrence of an electron-transfer process to produce the excited state with a smaller driving force as compared with a process to produce the ground state with a much larger driving force is a clear indication of the occurrence of a Marcus inverted region where the ET rate (k_{et}) decreases as the ET driving force ($-\Delta G_{et}^0$) increases for the strongly exergonic region ($-\Delta G_{et}^0 < \lambda$).[37] The Marcus *inverted* region has been, after a long controversy, well-established through studies on a number of donor/acceptor systems with fixed distances.[38−42] In *inter*molecular ET reactions, decisive evidence for the *inverted* region has, however, been scarce.[43] The chemiluminescence observed in electron transfer from BNAH to $Ru(bpy)_3^{3+}$ provides compelling evidence of the occurrence of the Marcus inverted region even for an *inter*molecular electron-transfer reaction.

When BNAH is replaced by 4-*t*-BuBNAH, no chemiluminescence due to $Ru(bpy)_3^{2+*}$ has been observed in the electron transfer from 4-*t*-BuBNAH to $Ru(bpy)_3^{3+}$. This is again ascribed to the facile C−C bond cleavage in 4-*t*-BuBNAH$^{\bullet+}$ (Scheme 3). Electron transfer from *t*-Bu$^\bullet$ (E_{ox}^0 vs SCE = 0.09 V)[31] to $Ru(bpy)_3^{3+}$ (E_{red}^0 vs SCE = 1.24 V)[29] is not exergonic enough to produce $Ru(bpy)_3^{2+*}$.

Formation of Radical Cations of NADH Analogues via Photoinduced Electron Transfer. The singlet excited state of BNAH (^{1}BNAH*) can act as an extremely strong electron donor judging from the highly negative one-electron oxidation potential (E_{ox}^{0*} vs SCE = −2.60 V).[5b] An electron transfer from ^{1}BNAH* to $CHBr_3$ (E_{red}^0 vs SCE = −1.55 V)[44] is highly exergonic ($\Delta G_{et}^0 = -1.05$ eV). Thus, laser excitation of an EtCN solution of BNAH and bromoform ($CHBr_3$) results in photoinduced electron transfer from ^{1}BNAH* to $CHBr_3$ to produce BNAH$^{\bullet+}$ (eq 1).

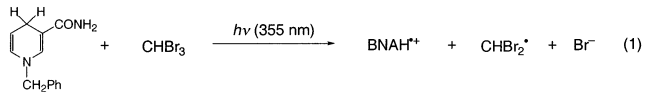

The transient absorption spectra in the visible region are observed by the laser flash photolysis of a deaerated EtCN solution of BNAH (4.0×10^{-4} M) and $CHBr_3$ (0.25 M) with 355 nm laser light as shown in Figure 8a. The new absorption appears at $\lambda_{max} = 460$ nm upon the laser excitation, and the decay of this absorption band is accompanied by the appearance of a new absorption band at 400 nm with isosbestic points. The rate of disappearance of the absorption band at 460 nm obeys first-order kinetics (see Supporting Information S4), coinciding with the rate of appearance of the absorption band at 400 nm (Figure 8b). Virtually the same transient absorption spectra were observed in the photoinduced electron transfer from 4-EtBNAH to $CHBr_3$ (see Supporting Information S5).

When BNAH is replaced by 4-*t*-BuBNAH where the hydrogen at the C(4) position is substituted by a *tert*-butyl group, no

(37) (a) Marcus, R. A. *Annu. Rev. Phys. Chem.* **1964**, *15*, 155. (b) Marcus, R. A.; Sutin, N. *Biochim. Biophys. Acta* **1985**, *811*, 265. (c) Marcus, R. A. *Angew. Chem., Int. Ed. Engl.* **1993**, *32*, 1111.
(38) (a) Miller, J. R.; Calcaterra, L. T.; Closs, G. L. *J. Am. Chem. Soc.* **1984**, *106*, 3047. (b) Closs, G. L.; Miller, J. R. *Science* **1988**, *240*, 440. (c) Gould, I. R.; Farid, S. *Acc. Chem. Res.* **1996**, *29*, 522. (d) McLendon, G. *Acc. Chem. Res.* **1988**, *21*, 160. (e) Winkler, J. R.; Gray, H. B. *Chem. Rev.* **1992**, *92*, 369. (f) McLendon, G.; Hake, R. *Chem. Rev.* **1992**, *92*, 481.
(39) Mataga, N.; Miyasaka, H. In *Electron Transfer from Isolated Molecules to Biomolecules Part 2*; Jortner, J., Bixon, M., Eds.; Wiley: New York, 1999; p 431.
(40) (a) Osuka, A.; Noya, G.; Taniguchi, S.; Okada, T.; Nishimura, Y.; Yamazaki, I.; Mataga, N. *Chem.-Eur. J.* **2000**, *6*, 33. (b) Mataga, N.; Chosrowjan, H.; Shibata, Y.; Yoshida, N.; Osuka, A.; Kikuzawa, T.; Okada, T. *J. Am. Chem. Soc.* **2001**, *123*, 12422.
(41) (a) Imahori, H.; Tamaki, K.; Guldi, D. M.; Luo, C.; Fujitsuka, M.; Ito, O.; Sakata, Y.; Fukuzumi, S. *J. Am. Chem. Soc.* **2001**, *123*, 2607. (b) Fukuzumi, S.; Guldi, D. M. In *Electron Transfer in Chemistry*; Balzani, V., Ed.; Wiley-VCH: Weinheim, 2001; Vol. 2, pp 270−337. (c) Imahori, H.; Guldi, D. M.; Tamaki, K.; Yoshida, Y.; Luo, C.; Sakata, Y.; Fukuzumi, S. *J. Am. Chem. Soc.* **2001**, *123*, 6617. (d) Fukuzumi, S.; Ohkubo, K.; Imahori, H.; Shao, J.; Ou, Z.; Zheng, G.; Chen, Y.; Pandey, P. K.; Fujitsuka, M.; Ito, O.; Kadish, K. M. *J. Am. Chem. Soc.* **2001**, *123*, 10676. (e) Fukuzumi, S.; Yoshida, Y.; Urano, T.; Suenobu, T.; Imahori, H. *J. Am. Chem. Soc.* **2001**, *123*, 11331.
(42) (a) Gust, D.; Moore, T. A. In *The Porphyrin Handbook*; Kadish, K. M., Smith, K. M., Guilard, R., Eds.; Academic Press: San Diego, CA, 2000; Vol. 8, pp 153−190. (b) Gust, D.; Moore, T. A.; Moore, A. L. *Acc. Chem. Res.* **2001**, *34*, 40. (c) Paddon-Row, M. N. *Acc. Chem. Res.* **1994**, *27*, 18. (d) Verhoeven, J. W. In *Electron Transfer-From Isolated Molecules to Biomolecules*; Jortner, J., Bixon, M., Eds.; John Wiley & Sons: New York, 1999; Part 1, pp 603−644.
(43) There have been considerable discussions on the reasons for the non-observance in the *inter*molecular electron-transfer reactions, see: (a) Weller, A.; Zachariasse, K. *Chem. Phys. Lett.* **1971**, *10*, 590. (b) Suppan, P. *Top. Curr. Chem.* **1992**, *163*, 95. (c) Efrima, S.; Bixon, M. *Chem. Phys. Lett.* **1974**, *25*, 34. (d) Brunschwig, B. S.; Ehrenson, S.; Sutin, N. *J. Am. Chem. Soc.* **1984**, *106*, 6858. (e) Barzykin, A. V.; Frantsuzov, P. A.; Seki, K.; Tachiya, M. *Adv. Chem. Phys.* **2002**, *123*, 511 and references therein.
(44) Bonesi, S. M.; Erra-Balsells, R. *J. Chem. Soc., Perkin Trans. 2* **2000**, 1583.

Scheme 5

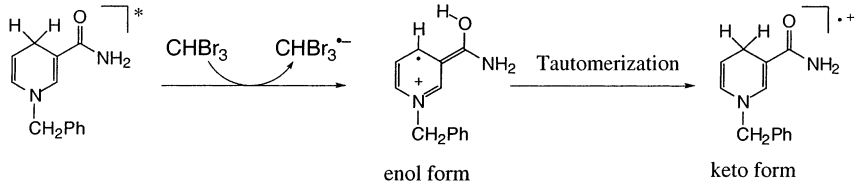

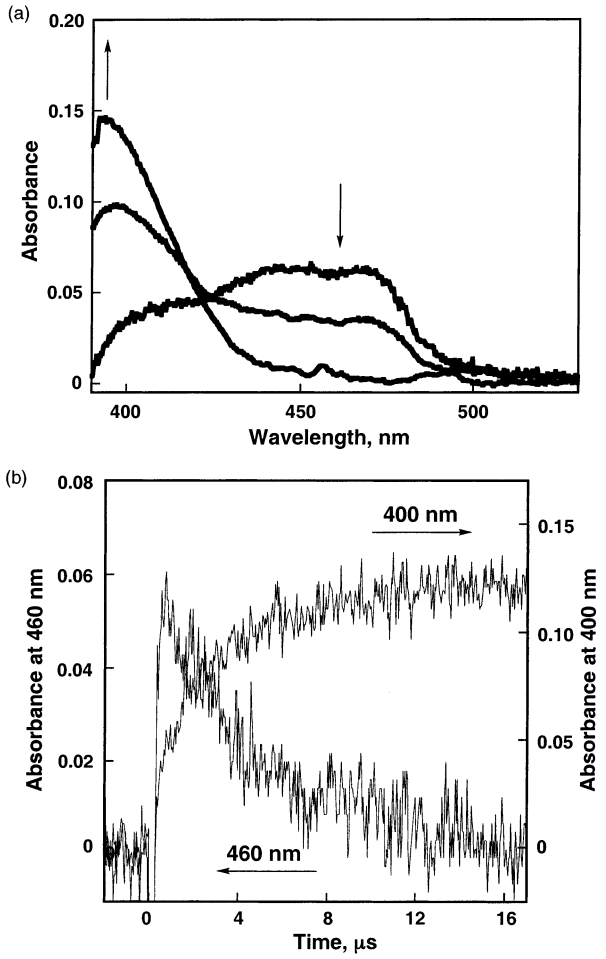

Figure 8. (a) Transient absorption spectra for the photoinduced electron transfer from ^{1}BNAH* (4.0×10^{-4} M) to $CHBr_3$ (0.25 M) in deaerated EtCN at 298 K (0.5, 3, and 10 μs after irradiation of laser pulse at $\lambda = 355$ nm with 20 mJ/pulse). (b) Time courses of the absorption change at 400 and 460 nm.

absorption band appears in the visible region (see Supporting Information S6) due to the facile and ultrafast C−C bond cleavage in 4-*t*-BuBNAH$^{\bullet+}$.

Because the observed absorption band at 400 nm in Figure 8a is overlapped with bleaching of the absorption band due to BNAH, this absorption band is virtually the same as the absorption band at 380 nm due to the keto form of BNAH$^{\bullet+}$ observed in the thermal electron transfer from BNAH to $Ru(bpy)_3^{3+}$ (Figure 1) and $Fe(bpy)_3^{3+}$.[18] Thus, the absorption band observed initially at 460 nm is assigned to the enol form of BNAH$^{\bullet+}$. In the highly exergonic electron transfer from ^{1}BNAH* to $CHBr_3$, the enol form of BNAH$^{\bullet+}$, which is higher in energy than the keto form, may be formed initially, followed by the conversion to the thermodynamically more stable keto form of BNAH$^{\bullet+}$ ($\lambda_{max} = 400$ nm) as shown in Scheme 5.[45]

The absorption band due to the enol form of BNAH$^{\bullet+}$ ($\lambda_{max} = 460$ nm) in MeCN is significantly red-shifted from that of

Table 3. Rate Constant (k) of Tautomerization of BNAH$^{\bullet+}$ and BNAH-4,4′-$d_2$$^{\bullet+}$ in Deaerated EtCN and the Kinetic Deuterium Isotope Effect (k_H/k_D)

T, K	10^{-5} k_H, s^{-1}	10^{-5} k_D, s^{-1}	k_H/k_D
298	3.2	1.7	1.9
283	2.7	1.2	2.2
268	2.2	0.9	2.4
243	1.6	0.5	3.2
228	1.2	0.3	4.1

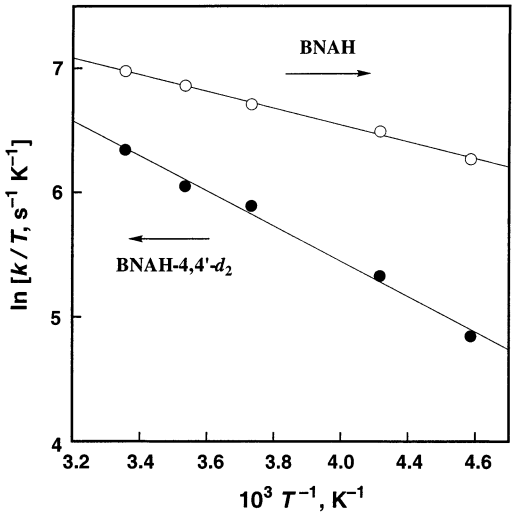

Figure 9. Eyring plots of the keto−enol tautomerization rate constant (k) of BNAH$^{\bullet+}$ (○) and BNAH-4,4′-$d_2$$^{\bullet+}$ (●) in deaerated EtCN.

the keto form (380 nm), being closer to the reported absorption band of NADH$^{\bullet+}$ ($\lambda_{max} = 540$ nm) produced by the biphotonic laser excitation of NADH in an aqueous solution.[12,46] Thus, the NADH$^{\bullet+}$ generated in such a high energy process may also be the enol form. However, the definitive assignment of NADH$^{\bullet+}$ has yet to be made.[47]

The conversion from the enol form to the keto form of BNAH$^{\bullet+}$ is intramolecular proton transfer. In such a case, kinetic isotope effects are expected to be observed. This is confirmed by determining the conversion rate from the enol form to the keto form using BNAH-4,4′-d_2. The rate constants of intramolecular proton transfer of BNAH$^{\bullet+}$ (k_H) and BNAH-4,4′-$d_2$$^{\bullet+}$ (k_D) were determined from the decay of the absorption band at

(45) The DFT calculations indicate that the enol form of BNAH$^{\bullet+}$ is by 3.9 kcal mol^{-1} more stable than the keto form, consistent with the result in the gas phase.[10,11] The observed conversion from the enol to the keto form in solution suggests that the keto form is more stabilized by solvation than the enol form.

(46) The absorption maximum at 460 nm observed in Figure 8a is different from that reported previously.[13] However, the assignment in our study is supported by the detailed dynamics and the kinetic isotope effects and also by the results in thermal electron-transfer reactions, monitored by the ESR and transient absorption spectra. The difference in solvents (H_2O and MeCN) may cause the difference in the absorption spectra of NADH$^{\bullet+}$ and BNAH$^{\bullet+}$.

(47) We could not detect NADH$^{\bullet+}$ in the electron-transfer oxidation of NADH by $Fe(bpy)_3^{3+}$ in an aqueous solution because of the instability of NADH$^{\bullet+}$ even by using a stopped-flow technique.

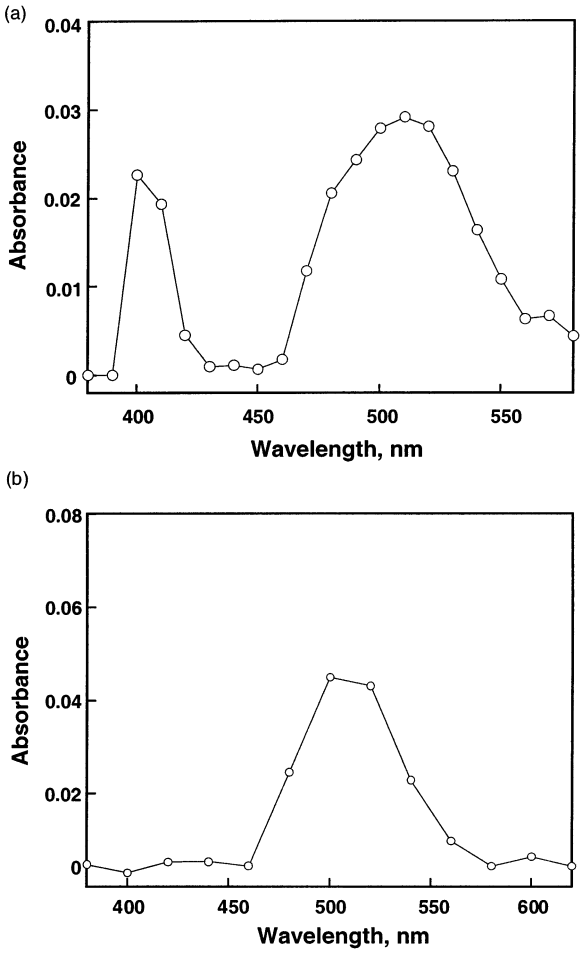

Figure 10. (a) Transient absorption spectra in photoinduced electron transfer from BNAH (3.0×10^{-3} M) to $Ru(bpy)_3^{2+*}$ (1.0×10^{-4} M) and (b) transient absorption spectra in photoinduced electron transfer from 4-*t*-BuBNAH (1.0×10^{-2} M) to $Ru(bpy)_3^{2+*}$ (1.0×10^{-4} M) in deaerated MeCN at 298 K (2 μs after irradiation of laser pulse at $\lambda = 450$ nm with 10 mJ/pulse).

460 nm or the appearance of the absorption band at 400 nm at various temperatures. The results are summarized in Table 3. The kinetic isotope effects (k_H/k_D) increase with a decrease in the temperature. The Eyring plots of the intramolecular proton transfer of $BNAH^{\bullet+}$ and BNAH-4,4′-$d_2^{\bullet+}$ are shown in Figure 9. The activation parameters obtained from the Eyring plots are listed in Table 2.

Photoinduced electron transfer from BNAH to the excited state of $Ru(bpy)_3^{2+}$ ($Ru(bpy)_3^{2+*}$) was also examined. The transient absorption spectrum is observed by the laser flash photolysis of a deaerated MeCN solution of BNAH (3.0×10^{-3} M) and $Ru(bpy)_3^{2+}$ (1.0×10^{-4} M) with 450 nm laser light as shown in Figure 10a. At 2 μs after the laser excitation, only the absorption band at 400 nm due to the keto form is observed together with the absorption band at 510 nm due to $Ru(bpy)_3^{+}$,[48] produced in the electron transfer from BNAH to $Ru(bpy)_3^{2+*}$. The electron transfer from BNAH to $Ru(bpy)_3^{2+*}$ is slightly exergonic ($\Delta G_{et}^0 = -0.22$ eV);[5b] therefore, the keto form of $BNAH^{\bullet+}$ is produced directly in contrast with the case of the highly exergonic electron transfer from $^1BNAH^*$ to $CHBr_3$.

When BNAH is replaced by 4-*t*-BuBNAH, only the absorption band at 510 nm due to $Ru(bpy)_3^{+}$ is observed as shown in Figure 10b where no transient absorption spectrum due to 4-*t*-$BuBNAH^{\bullet+}$ is detected due to the facile C−C bond cleavage in 4-*t*-$BuBNAH^{\bullet+}$ (Scheme 2).

Summary and Conclusions

In this study, we present the first direct detection of radical cations of NADH analogues by ESR. The ESR spectra have clearly shown that the radical cation is the keto form. This indicates that the keto form of $BNAH^{\bullet+}$ is more stable than the enol form of $BNAH^{\bullet+}$ in solution, which is opposite to the case in the gas phase.[10,11] The enol form of $BNAH^{\bullet+}$ was observed only in the case of highly exergonic electron transfer in which direct production of the keto form of $BNAH^{\bullet+}$ is unfavorable. The observation of chemiluminescence when BNAH is oxidized by $Ru(bpy)_3^{3+}$ indicates that $BNA^{\bullet}$ is formed by deprotonation of $BNAH^{\bullet+}$.

Acknowledgment. This work was partially supported by Grants-in-Aid for Scientific Research on Priority Area (Nos. 11228205, 13440216, and 14045249) from the Ministry of Education, Culture, Sports, Science, and Technology, Japan.

Supporting Information Available: Spectral change in the reaction between BNAH and $Ru(bpy)_3^{3+}$ (S1), spectral change in the reaction between 4-*t*-BuBNAH and $Fe(bpy)_3^{3+}$ (S2), the first-order plots in the reaction between BNAH and $Ru(bpy)_3^{3+}$ (S3), the first-order plots in photoinduced electron transfer from $^1BNAH^*$ to $CHBr_3$ (S4), transient absorption spectra in photoinduced electron transfer from ^{1}4-EtBNAH* to $CHBr_3$ (S5), transient absorption spectra in photoinduced electron transfer from ^{1}4-*t*-$BuBNAH^*$ to $CHBr_3$ (S6) (PDF). This material is available free of charge via the Internet at http://pubs.acs.org.

JA029623Y

(48) Baxendale, J. H.; Fiti, M. *J. Chem. Soc., Dalton Trans.* **1972**, 1995.